JOURNAL OF MATERIALS SCIENCE **34** (1999) 6063–6068

Structural and magnetic properties of MnO-B_2O_3-SrO glasses

I. ARDELEAN, M. PETEANU, V. SIMON
Faculty of Physics, Babes-Bolyai University, 3400 Cluj-Napoca, Romania
E-mail: arde@phys.ubbcluj.ro

S. FILIP, M. FLORA
Department of Physics, University of Oradea, 3700 Oradea, Romania

S. SIMON
Faculty of Physics, Babes-Bolyai University, 3400 Cluj-Napoca, Romania

The Mn^{2+} ion distribution in different structural units in $2B_2O_3{\cdot}SrO$ glasses was revealed by means of electron paramagnetic resonance measurements. Octahedral symmetric sites, tetragonally distorted, were detected and also the progressive clustering of Mn^{2+} ions above a certain impurity level ($x \geq 10$ mol % MnO). Magnetic measurements revealed that both Mn^{2+} and Mn^{3+} ionic species are simultaneously present in the matrix and that a transition from magnetically isolated ions to antiferromagnetically coupled pairs occurs on increasing the manganese content over 10 mol % MnO.

1. Introduction

Manganese ions have been frequently used as paramagnetic probes for exploring the structure and properties of vitreous systems. Many oxide glasses such as borate [1–5], alkali-silicate [6, 7], aluminum-silicate or phosphate [8], tellurite [9, 10] and also chalcogenide [11–13] or halide glasses [14–16] have been investigated by means of electron paramagnetic resonance (EPR) due to Mn^{2+} ions. A special effort was made to develop a theoretical description for explaining the resonance lines at $g \cong 4.3$ and $g \cong 3.3$ in Mn^{2+} absorption spectra. Valuable information has been obtained concerning the structural details of glasses, from the paramagnetic Mn^{2+} ion distribution in different structural units building the network, their coordination, the valence state of manganese ions, etc.

NMR was successfully used in revealing the structural details of binary MnO-B_2O_3 glasses [17].

The magnetic properties of glasses containing manganese has been investigated in lead-, [18], potassium-, [5] and lithium [19] -borate vitreous systems, and also in TeO_2-B_2O_3-PbO [20] and Bi_2O_3-GeO_2 [21]. The type and strength of interactions concerning manganese were determined in various concentration ranges. Besides Mn^{2+} ions, the Mn^{3+} ionic species are often detected [18–20].

Strontium borate glasses have been studied by means of EPR [4], and also by ^{11}B nuclear magnetic resonance [22, 23], infrared spectroscopy and hardness measurements [23].

This paper aims to present our results concerning the structural details of the $2B_2O_3{\cdot}SrO$ vitreous matrix revealed by the distribution of manganese ions on various structural aggregates, their valence states and the magnetic interactions involving them. Investigations were made by means of EPR and magnetic susceptibility measurements.

2. Experimental

Glasses of the system $x\text{MnO}{\cdot}(100 - x)[2B_2O_3{\cdot}\text{SrO}]$ have been prepared in the composition range $0 \leq x \leq 50$ mol % by using reagent grade $MnCO_3$, H_3BO_3 and $SrCO_3$. The mixtures, in suitable proportions corresponding to the desired concentration of MnO, were mechanically homogenized and melted in sintered corundum crucibles in an electric furnace at 1250 °C. The molten material was kept at this temperature for 30 min to homogenize by means of thermal convection, then quenched at room temperature by pouring onto a stainless-steel plate. Typical glasses in both aspect and structure were obtained, having a gradual coloration specific to manganese within the investigated concentration range.

The structure of samples was analyzed by means of X-ray diffraction. The patterns obtained did not reveal any crystalline phase in the glasses.

The EPR measurements were performed on powder samples at room temperature by using JEOL-type equipment with 100 KHz field modulation in the X frequency band. The resonance line width was measured with an error of ± 0.7 mT and the g values were calculated with an error of ± 0.002.

The magnetic susceptibility measurements were performed using a Faraday-type balance, in the 80–300 K temperature range.

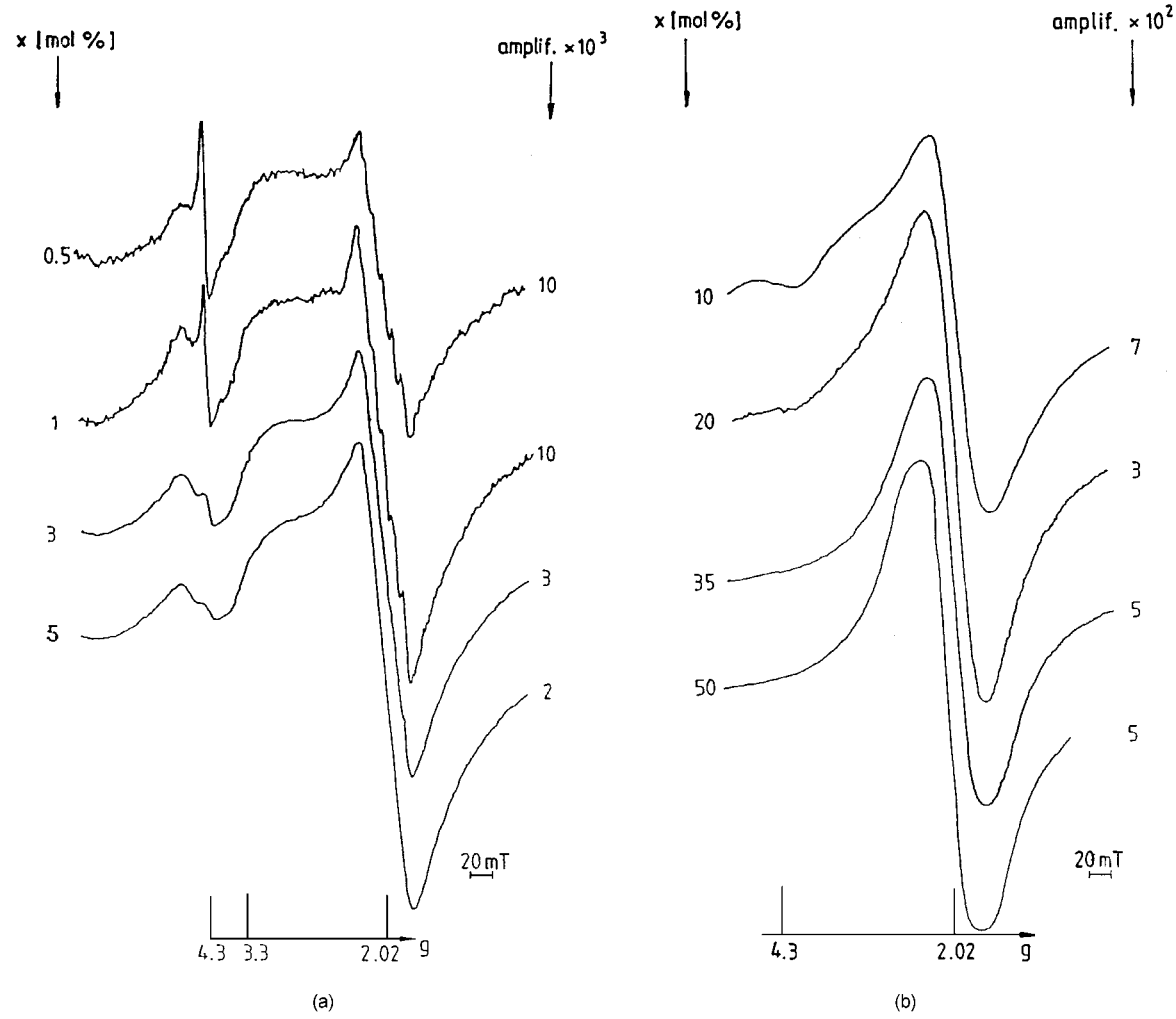

Figure 1 EPR absorption spectra of Mn^{2+} ions in glass matrix $2B_2O_3{\cdot}SrO$ at low MnO content (a), and for high concentrations of MnO (b).

3. Results

3.1. EPR measurements

For all concentrations, the EPR absorption spectra obtained, show resonance lines due to Mn^{2+} ($3d^5$; $^6S_{5/2}$) paramagnetic ions. The structure of the absorption spectra strongly depends on the MnO content of the sample, as may be observed in Fig. 1. At low concentrations of Mn^{2+}, the spectrum consists of absorptions centered at effective g factors of 4.30, 3.33 and 2.02. The absorption at $g \cong 2.02$ is the prevalent line of the spectrum, having hyperfine structure (hfs) characteristic of the ^{55}Mn ($I = 5/2$) isotope that is well resolved for samples with $0.5 \leq x \leq 3$ mol % (Fig. 1a). At high manganese content, the spectrum reduces to a single absorption line, without hfs, centered at $g \cong 2.0$ (Fig. 1b).

The absorption with $g \cong 4.3$ is less intense and does not show hfs. The line is broadened due to the unresolved hfs. Its intensity increases in the $0.5 \leq x \leq 10$ mol % range and then decreases to zero. Superimposed on this broad absorption, a line corresponding to accidental impurities of Fe^{3+} ($3d^5$; $^6S_{5/2}$) ions was also detected (Fig. 1a). Being narrow and well resolved, this line has been used as a spectrum field marker being characterized by the well known $g = 4.285$ value [24].

The absorption centered at $g \cong 3.33$ was detected in the $0.5 \leq x \leq 10$ mol % range. It is a broad unresolved line and does not show hfs.

As previously mentioned, only the $g \cong 2.02$ absorption shows well resolved hfs. The resolution depends on the Mn^{2+} ions concentration, as may be seen in Fig. 2. The best resolution was obtained at the lowest limit of paramagnetic ions concentration range, providing the optimal opportunity in positioning the lines of the hfs sextet, and estimating the EPR parameters of the absorption line. The hyperfine coupling constant, A, was approximated as separation between the lines of the central pair of the hfs sextet, and the g factor was calculated at the middle point of this. For the sample having $x = 0.5$ mol % MnO these parameters were estimated as $A = 7.7 \pm 1.1$ mT and $g = 2.0170 \pm 0.0067$. The separation between the hfs lines, ΔH_{hfs}, increases with the magnetic field (Fig. 2). This suggests second order terms to be taken into account in the spin Hamiltonian in an accurate theoretical approach.

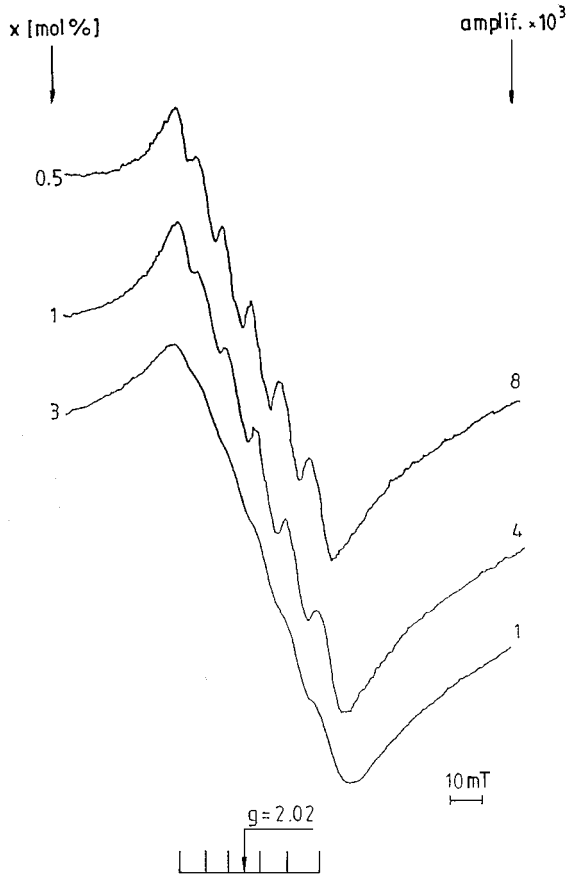

Figure 2 The evolution of the hyperfine structure of the $g \cong 2.02$ EPR absorption when increasing the Mn^{2+} ions concentration.

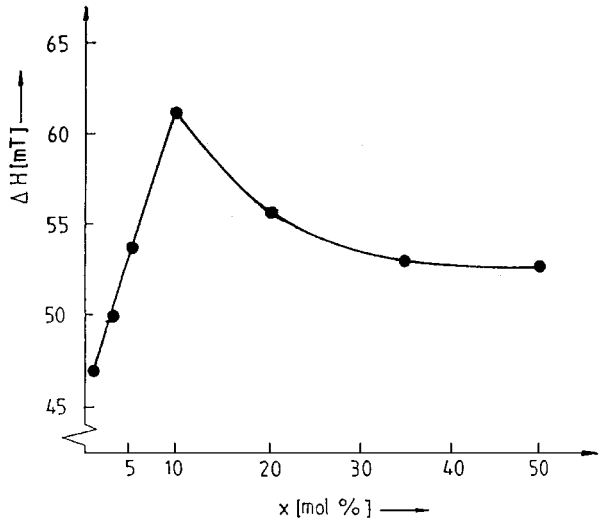

Figure 3 The composition dependence of the peak-to-peak line width of the $g \cong 2.0$ absorption.

The hfs sextet superimposes on a large absorption line, the envelope of all contributions having $g \cong 2.0$. This line also depends on the manganese content of the sample. The concentration dependence of its line-width is presented in Fig. 3 (the smooth curve is a guide to the eye) and has a complex evolution.

3.2. Magnetic susceptibility data

The temperature dependence of the reciprocal magnetic susceptibility of some of the studied strontium-borate glasses is presented in Fig. 4. For samples containing $x \leq 10$ mol % MnO the magnetic susceptibility obeys

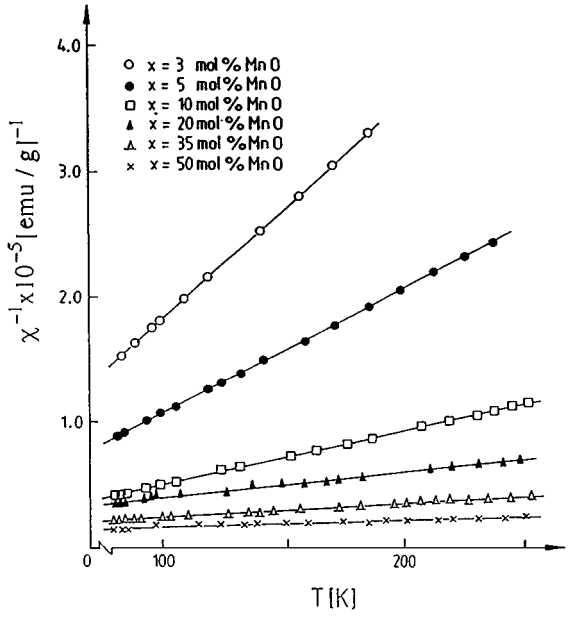

Figure 4 Temperature dependence of the reciprocal magnetic susceptibility of glasses in the system xMnO·$(100-x)$[$2B_2O_3$·SrO].

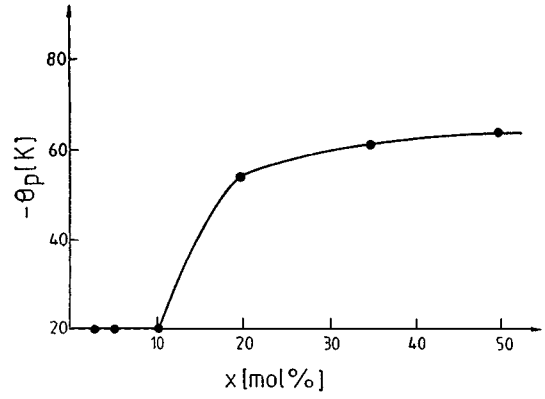

Figure 5 The dependence of the paramagnetic Curie temperature on the MnO content of samples in the system xMnO·$(100-x)$[$2B_2O_3$·SrO].

a Curie law, $\chi = C/T$, while for higher concentrations of manganese a Curie-Weiss law, $\chi = C/(T-\theta_p)$, with negative paramagnetic Curie temperature, θ_p, was followed.

The dependence of the paramagnetic Curie temperature on the MnO content of the samples is given in Fig. 5. The absolute value of θ_p increases non-linearly with the manganese ions content increasing.

For a correct estimation of the Curie constant values, C, and the effective magnetic moments, μ_{eff}, corrections due to the diamagnetism of the vitreous matrix and MnO were taken into account. In Fig. 6 is presented the composition dependence of the molar Curie constant.

The effective magnetic moment of manganese ions was calculated as $\mu_{eff} = 2.827\sqrt{C_M/x}$. For samples having $x \leq 10$ mol % the value $\mu_{eff} = 5.92\,\mu_B$ was obtained, which is very close to that corresponding to free Mn^{2+} ions. For $x > 10$ mol % the obtained μ_{eff} values may be justified only by the simultaneous presence of both Mn^{2+} and Mn^{3+} ionic species. Therefore, the molar fractions of these ions were estimated in first approximation by using the relations:

TABLE I Molar fractions of the Mn^{2+} and Mn^{3+} ions in glasses of the system xMnO·$(100-x)$[$2B_2O_3$·SrO]. The composition errors are ±0.2 mol %

x (mol % MnO)	x_1 (mol % Mn^{2+}O)	x_2 (mol % Mn^{3+}O)
3.0	3.0	0.0
5.0	5.0	0.0
10.0	10.0	0.0
20.0	15.0	5.0
35.0	12.3	22.7
50.0	6.3	43.7

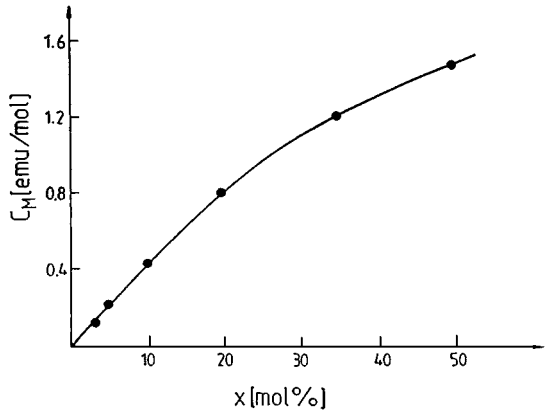

Figure 6 Composition dependence of the molar Curie constant.

$$x\mu_{\text{exp}}^2 = x_1\mu_{\text{Mn}^{2+}}^2 + x_2\mu_{\text{Mn}^{3+}}^2,$$
$$x = x_1 + x_2,$$

where μ_{exp} is the effective magnetic moment determined experimentally from the temperature variation of the magnetic susceptibility, x_1 and x_2 are the molar fractions of Mn^{2+} and Mn^{3+} ionic species and $\mu_{\text{Mn}^{2+}} = 5.92\,\mu_B$, $\mu_{\text{Mn}^{3+}} = 4.90\,\mu_B$ are the values of the magnetic moment corresponding to the free Mn^{2+} and Mn^{3+} ions, respectively. The results obtained are listed in Table I. The molar fraction of Mn^{2+} ions increases with MnO content up to $x = 20$ mol %, then decreases. The molar fraction of Mn^{3+} ions is different of zero only for samples with $x \geq 20$ mol % MnO, their values exceeding those corresponding to Mn^{2+} ions for $x \geq 35$ mol % MnO.

4. Discussion

The recorded EPR absorption spectra are due to the Mn^{2+} paramagnetic ions evidenced as ionic species within the investigated concentration range.

The $g \cong 2.0$ absorption line was generally attributed to isolated paramagnetic centers in octahedral symmetric sites slightly tetragonally distorted, or to exchange-coupled pairs of ions [25]. Depending on concentration, our samples show an evolution of the vitreous matrix structure from structural units involving Mn^{2+} in well defined vicinities having a certain symmetry, to structural aggregates containing clustered ionic formations. This evolution was revealed by the changes in the $g \cong 2.02$ absorption line when increasing the Mn^{2+} ions concentration (Fig. 1).

Within the low concentration range, the $g \cong 2.02$ absorption line, which is the prevalent feature of the spectrum, has a resolved hfs (Fig. 1a). The hyperfine sextet is due to isolated Mn^{2+} ions in high symmetric sites (octahedral) that are separated well enough from each other to avoid strong dipolar interactions. The g factor and hyperfine coupling constant values and the well resolved hfs support this statement and also evidence the predominantly ionic character of the bonding between Mn^{2+} and the O^{2-} ions generating the octahedral symmetric ligand field. There are weak axial distortions superimposed on this field varying from one vicinity to another [26, 27]. Their random orientation determines the broadening of the absorption line. The random distribution of Mn^{2+} ions in the vitreous matrix, together with this broadening, results in a large background line that is the envelope of all contributions at $g \cong 2.0$ having superimposed the hfs sextet.

When the paramagnetic ions concentration increases, the hfs smears out and the intensity of the symmetric absorption line at $g \cong 2.0$ increases. Its linewidth follows the variation presented in Fig. 3. Within $0.5 \leq x \leq 10$ mol % MnO the line progressively broadens evidencing dipole-dipole type interactions between the Mn^{2+} ions. For $x > 10$ mol % MnO the line suddenly narrows, evidencing magnetic exchange-type mechanisms between the Mn^{2+} ions, close enough to each other for interacting. The reached doping level of the matrix imposes the progressive clustering of Mn^{2+} ions. For $x > 25$ mol % MnO the narrowing is balanced by broadening effects due to another mechanisms so as the interaction between mixed valence states of manganese, or the progressive disordering of the vitreous system. At high MnO content, besides the Mn^{2+} ions species, the only ones giving rise to EPR absorption in our experiment, superior valance states may occur in the sample. In vitreous oxide matrices, Mn^{3+} ions have been frequently reported as progressively involved when increasing the MnO content [18–20].

There are also strongly distorted sites of Mn^{2+} ions in octahedral vicinities subjected to strong crystal field effects. These give rise to absorption lines at $g \cong 4.3$ and $g \cong 3.3$ (Fig. 1a). These resonance lines are less intense and their hfs is unresolved. There is a relative small concentration of Mn^{2+} ions involved in such structural units. The absorption lines at $g \cong 4.3$ and $g \cong 3.3$ reach their maximum intensity at about 5 mol % MnO. The increase in the MnO content reduces the possibility for Mn^{2+} to structure their vicinity so that structural units involving Mn^{2+} in low symmetric crystal field sites become less well represented and the paramagnetic ions are gradually involved in clusters. This clustering process generalizes for concentrations exceeding 10 mol % MnO.

The lack of hfs at the $g \cong 4.3$ and $g \cong 3.3$ absorption lines is due to fluctuations of the ligand field parameters in the paramagnetic ion neighbourhood and the random distribution of the octahedral vicinity distortions [15]. Some of the low-symmetric centers no longer contribute to the isotropic absorption and the resulting EPR line is broadened due to anisotropy and the ligand parameters distribution [28].

From the variety of symmetries efficient in splitting the $^6S_{5/2}$ state the tetragonal and tetragonally distorted cubic vicinities are of particular interest and give theoretical isotropic g_{eff} values of 4.285 and 3.33 very close to those experimentally detected [28]. These values correspond to transitions within the lowest Kramers doublet, in the strong ligand field approximation.

The magnetic behaviour revealed by the dependencies in Fig. 4 show manganese ions as isolated, but involved in dipole-dipole type interactions, in agreement with the $g \cong 2.0$ line broadening for samples with $x \leq 10$ mol % MnO. For concentrations $x > 10$ mol % MnO, the manganese ions are involved in superexchange interactions and are antiferromagnetically coupled, as indicate the negative values obtained for θ_p. These interactions result in the EPR line at $g \cong 2.0$ narrowing for samples with $x \geq 10$ mol % MnO.

The non-linear dependence of the paramagnetic Curie temperature, θ_p, with the MnO content increasing, given in Fig. 5, suggests, after a certain impurifying level, the presence of Mn^{3+} ions besides the Mn^{2+} ions. This was confirmed by the values of C_M experimentally obtained. For $x > 10$ mol %, the C_M values are smaller than those corresponding to the case when all manganese would enter as Mn^{2+} species, but higher than those calculated for the case when all ions would be the Mn^{3+} species. The simultaneous presence of both Mn^{2+} and Mn^{3+} ions at high MnO content (Table I) explains some of the above mentioned peculiarities of the EPR absorption spectra.

According to [17] MnO acts as glass network modifier in the binary MnO-B_2O_3 system, like Na_2O, K_2O or Li_2O, and manganese ions occur in the (2+) valence state. The proportion of MnO in our strontium-borate glasses determine the structural behaviour of manganese ions. The strontium oxide is a glass network modifier in this system, and consequently only a part of manganese ions having the (2+) valence state are disposed in sites of network modifier. The other part of manganese ions, having the (3+) valence state, are probably disposed in sites of network former, like boron, in the matrix.

By comparing the obtained results concerning strontium-borate systems with those previously obtained for manganese containing $[2B_2O_3 \cdot K_2O]$ glass matrix [5] we find that the EPR absorption line is narrower for the potassium-borate glasses than for the strontium-borate ones, at the same MnO content, and consequently the magnetic interactions involving manganese ions are stronger. K_2O containing glasses show nearly constant line-width of about 43.5 mT in the 10–30 mol % MnO range, while the $\Delta H = f(x)$ dependence show a maximum of about 61 mT at $x = 10$ mol % MnO for the SrO containing system. This behaviour reflects different manganese ions ordering in the two systems. The Mn^{3+} species were detected beginning on 10% MnO in potassium-borate glasses, whereas in the strontium-borate glasses there are Mn^{3+} detectable concentrations only for $x \geq 20$ mol % MnO. There are indirect influences on the line width of the Mn^{2+} ions spectrum due to Mn^{2+}-Mn^{3+} interactions which broaden the resonance line. The mixed valence pairs induce a structural rearrangement of the matrix, which differ in the two systems due to the different Mn^{3+} ions content. The magnetic behaviour of the two systems is also different. The K_2O containing glasses show superexchange magnetic interactions for samples with $x \geq 7$ mol % MnO, while the SrO containing ones show such interactions only for $x > 10$ mol % MnO.

There are different distributions of valence states of manganese ions in the MnO-B_2O_3 [17], xMnO·$(100-x)[2B_2O_3{\cdot}K_2O]$ [5] and xMnO·$(100-x)$ $[2B_2O_3{\cdot}SrO]$ vitreous systems. Similar to other transition metal ions having several ionic valence states, the chemical composition of glasses [29] and the conditions of preparation [30] may determine the valence states of manganese ions and their distribution on different sites of the vitreous matrix. Due to the presence of K_2O or SrO acting as network modifier the Mn^{3+} ionic species, simultaneously present with the Mn^{2+} ones, were also detected in the corresponding systems. Due to valence differences of K^+ and Sr^{2+} ions there are differences between the manganese ions distributions on different valence states and different structural units building the network, and consequently differences in the magnetic behaviour of glasses.

5. Conclusions

EPR absorptions due to Mn^{2+} ions were detected in xMnO·$(100-x)[2B_2O_3{\cdot}SrO]$ glasses within a large concentration range, i.e. $0.5 \leq x \leq 50$ mol % MnO.

The distribution of Mn^{2+} ions on several structural units of the vitreous matrix depends on the MnO content. In the low concentration range, $0.5 \leq x \leq 5$ mol % MnO, the Mn^{2+} ions were identified in sites of octahedral symmetry slightly tetragonally distorted. They give rise to intense absorption lines centred at $g \cong 2.02$ showing well resolved hyperfine structure up to 3 mol % MnO. There are also the strongly distorted versions of these sites, subjected to strong crystal field effects. Mn^{2+} ions in tetragonal sites give resonance lines at $g_{\text{eff}} \cong 4.3$ and $g_{\text{eff}} \cong 3.3$. Their intensity is small enough to indicate a relatively low concentration of Mn^{2+} ions involved in such structural units.

In the high concentration range, $10 < x \leq 50$ mol % MnO, the progressive clustering of Mn^{2+} ions was identified by the evolution of the corresponding absorption line at $g \cong 2.0$. Its line-width depends on concentration showing a dipolar broadening within $0.5 \leq x \leq 10$ mol % MnO, and a superexchange narrowing for $x \geq 10$ mol % MnO. The magnetic measurements evidenced a change in the temperature dependence of the reciprocal magnetic susceptibility from a Curie-type behaviour to a Curie-Weiss one, at concentrations of about 10 mol % MnO. Antiferromagnetic superexchange coupling between the manganese ions involved in clusters, was detected.

For samples with $x < 20$ mol % MnO both Curie constant and effective magnetic moment values confirm the presence of Mn^{2+} ionic species as a unique valence state. The values obtained for C_M and μ_{eff} for samples with $x \geq 20$ mol % MnO may be supported only

by admitting the simultaneous presence of both Mn^{2+} and Mn^{3+} valence states.

References

1. D. L. GRISCOM and R. E. GRISCOM, *J. Chem. Phys.* **47** (1967) 2711.
2. R. D. DOWSING and J. F. GIBSON, *ibid.* **50** (1969) 294.
3. A. V. DE WIJN and R. E. VAN BALDEREN, *ibid.* **46** (1967) 4.
4. P. C. TAYLOR and P. J. BRAY, *J. Chem. Phys. Solids* **33** (1972) 43.
5. I. ARDELEAN, GH. ILONCA and M. PETEANU, *Solid State Commun.* **52** (1984) 147.
6. H. H. WICKMAN, M. P. KLEIN and D. A. SHIRLEY, *J. Chem. Phys.* **42** (1965) 2113.
7. D. LOVERIDGE and S. PARKE, *Phys. Chem. Glasses* **12** (1971) 19.
8. J. W. H. SCHREURS, *J. Chem. Phys.* **69** (1978) 2151.
9. M. PETEANU, I. ARDELEAN and AL. NICULA, *Rev. Roum. Phys.* **28** (1983) 47.
10. I. ARDELEAN, M. PETEANU and GH. ILONCA, *Phys. Stat. Sol. a* **58** (1980) K33.
11. R. C. NICKLIN, C. P. POOLE and H. A. FARACH, *J. Chem. Phys.* **68** (1973) 2579.
12. V. N. LAZUKIN and I. V. CHEPELEVA, *DAN SSSR* **214** (1974) 787.
13. I. V. CHEPELEVA, E. A. ZHILINSKAJA, V. N. LAZUKIN, A. P. CERNOV and V. I. OLKHOVSKII, *Phys. Stat. Sol. b* **82** (1977) 189.
14. B. PETROVA, M. FRUMAR, E. CERNOSKOVA and V. CERNY, *J. Non-Cryst. Solids* **161** (1993) 316.
15. V. CERNY, B. PETROVA and M. FRUMAR, *ibid.* **125** (1990) 17.
16. V. CERNY, B. FRUMAROVA-PETROVA, J. ROSA, I. L. LIEHOLIT and M. FRUMAR, *ibid.* **192/193** (1995) 165.
17. M. J. PARK, P. J. BRAY and J. KOREAN, *Phys. Soc.* **14** (1981) 67.
18. GH. ILONCA, I. ARDELEAN and O. COZAR, *J. Physique* **49** (1988) 8.
19. I. ARDELEAN, GH. ILONCA and O. COZAR, *Rev. Roum. Phys.* **33** (1988) 179.
20. I. ARDELEAN, M. PETEANU, S. FILIP and D. ALEXANDRU, *J. Magn. Magn. Mat.* **157** (1996) 239.
21. I. ARDELEAN, M. PETEANU, S. FILIP, V. SIMON and I. TODOR, *J. Non-Cryst. Solids* in press.
22. M. J. PARK and P. J. BRAY, *Phys. Chem. Glasses* **13** (1972) 50.
23. S. J. MOON, M. S. KIM, S. J. CHUNG and H. T. KIM, *J. Korean Phys. Soc.* **29** (1996) 213.
24. T. CASTNER, G. S. NEWELL, W. C. HOLTON and C. P. SLICHTER, *J. Chem. Phys.* **32** (1960) 668.
25. D. L. GRISCOM, *J. Non-Cryst. Solids* **40** (1980) 211.
26. I. N. FEUERHELM, S. M. SIBLEY and W. A. SIBLEY, *J. Solid State Chem.* **54** (1984) 164.
27. J. L. RAO, B. SREEDHAR, Y. C. RATANAKAR and S. V. LAKSHMANN, *J. Non-Cryst. Sol.* **92** (1987) 175.
28. M. PETEANU and AL. NICULA, *Studii si Cercet. de Fizica* **33** (1981) 29; *ibid.* **34** (1982) 14.
29. E. BURZO, I. ARDELEAN and I. URSU, *J. Mater. Sci.* **15** (1980) 581.
30. E. BURZO, I. URSU, D. UNGUR and I. ARDELEAN, *Mat. Res. Bull.* **15** (1980) 1273.

Received 19 August 1998
and accepted 5 May 1999